MATERIALS SCIENCE

Metallo-alginate hydrogel can potentiate microwave tumor ablation for synergistic cancer treatment

Yujie Zhu, Zhijuan Yang, Zijian Pan, Yu Hao, Chunjie Wang, Ziliang Dong, Quguang Li, Yikai Han, Longlong Tian, Liangzhu Feng*, Zhuang Liu*

Microwave ablation (MWA) as a local tumor ablation strategy suffers from posttreatment tumor recurrence. Development of adjuvant biomaterials to potentiate MWA is therefore of practical significance. Here, the high concentration of Ca^{2+} fixed by alginate as Ca^{2+}-surplus alginate hydrogel shows enhanced heating efficiency and restricted heating zone under microwave exposure. The high concentration of extracellular Ca^{2+} synergizes with mild hyperthermia to induce immunogenic cell death by disrupting intracellular Ca^{2+} homeostasis. Resultantly, Ca^{2+}-surplus alginate hydrogel plus MWA can ablate different tumors on both mice and rabbits at reduced operation powers. This treatment can also elicit antitumor immunity, especially if synergized with Mn^{2+}, an activator of the stimulation of interferon genes pathway, to suppress the growth of both untreated distant tumors and rechallenged tumors. This work highlights that in situ–formed metallo-alginate hydrogel could act as microwave-susceptible and immunostimulatory biomaterial to reinforce the MWA therapy, promising for clinical translation.

INTRODUCTION

Microwave ablation (MWA) is an interventional technique developed for local thermal ablation of tumors by using the heat generated by the intense oscillation of polar molecules under microwave exposure (*1*, *2*). Attributing to its minimal invasiveness, short-term clinical performance, and highly effective cell killing capacity, MWA has currently been widely used for treating several types of solid tumors including hepatocellular carcinoma, pulmonary cancer, and colorectal cancer liver/pulmonary metastases (*3*). However, owing to the irregular shape of most tumors, current MWA treatment often needs to produce a larger ablation zone at a higher operation power density for complete tumor ablation and thereby would impose severe thermal damages to surrounding normal tissues with frequent side effects (e.g., post-ablation syndrome and pleural effusions) (*4*–*6*). Therefore, it is of great significance to find out a type of functional agent that can confer current MWA with enhanced tumor heating efficacy in a tunable heating zone to realize more efficient MWA cancer treatment with superior safety.

It has been found in both preclinical animal experiments and clinical practices that local thermal ablation including MWA treatment could create a large pool of tumor antigens and various damage-associated molecular patterns (DAMPs) to prime adaptive antitumor immunity. These immune responses, however, are often not effective enough to inhibit tumor metastases and recurrence (*7*, *8*), even in combination with other immunotherapeutics such as immune checkpoint blockade (*9*, *10*), mainly attributing to the immunosuppressive tumor microenvironments. Given that immunostimulatory adjuvants could potentiate different local thermal ablation treatments to synergistically suppress the tumor progression (*11*, *12*), it is, therefore, of great interests to develop adjuvant biomaterials with both profound microwave susceptibility and immunostimulatory effect for enhanced MWA ablation.

Metal ions can continuously reorient under the oscillating electromagnetic radiation and thus enable efficient microwave heating (*13*–*15*). Compared to bulk solutions, metal ions encapsulated within nanoscale or microscale structures have been found to be potent MWA susceptible agents with enhanced microwave heating owing to the spatial confinement effect (*16*–*19*). In addition, Ca^{2+} ions are known to play important roles in cell proliferation, apoptosis, and the activation of diverse immune cells (*20*–*22*). Recently, it has been reported that the disruption of intracellular Ca^{2+} hemostasis can result in effective cancer cell killing (*23*, *24*). Moreover, some recent studies have reported that some transition metal ions including manganese ions (Mn^{2+}) and zinc ions (Zn^{2+}) could efficiently prime the stimulator of interferon genes (STING) pathway via different mechanisms to elicit potent innate and adaptive antitumor immunities for effective tumor suppression (*25*–*27*). Inspired by those previous findings and the high coordination affinity of alginate to divalent metal ions, in our work here, we designed a metallo-alginate hydrogel to not only potentiate MWA but also enhance the antitumor immune responses after MWA treatment.

In this study, we first found that excess Ca^{2+} upon being fixed with sodium alginate as Ca^{2+}-surplus hydrogel could work as an efficient microwave susceptible agent to enable enhanced microwave heating in a Ca^{2+} concentration–dependent manner (Fig. 1). Treatment of increased extracellular Ca^{2+} (e.g., 4 mM) together with mild hyperthermia (43°C) could synergistically induce effective immunogenic cell death (ICD) of cancer cells by inducing intracellular Ca^{2+}-overloading and subsequent mitochondria dysfunction. Compared to microwave irradiation alone, the in situ–formed Ca^{2+}-surplus alginate hydrogel together with microwave irradiation could lead to more efficient tumor temperature increment, resulting in effective ablation of tumors in both mice and rabbits. Moreover, it was uncovered that this in situ–formed Ca^{2+}-surplus alginate hydrogel showed comparable immunostimulatory effect to that of imiquimod (R837), a commercial Toll-like receptor 7 (TLR7) agonist, in synergizing with microwave irradiation to suppress the growth of distant tumors. Furthermore, we demonstrated that intratumoral fixation of Ca^{2+}-surplus alginate hydrogel together with Mn^{2+} ions would remarkably improve the immune stimulatory effect of WMA

Institute of Functional Nano & Soft Materials (FUNSOM), Jiangsu Key Laboratory for Carbon-Based Functional Materials & Devices, Soochow University, 199 Ren'ai Road, Suzhou, 215123 Jiangsu, PR China.
*Corresponding author. Email: zliu@suda.edu.cn (Z.L.); lzfeng@suda.edu.cn (L.F.)

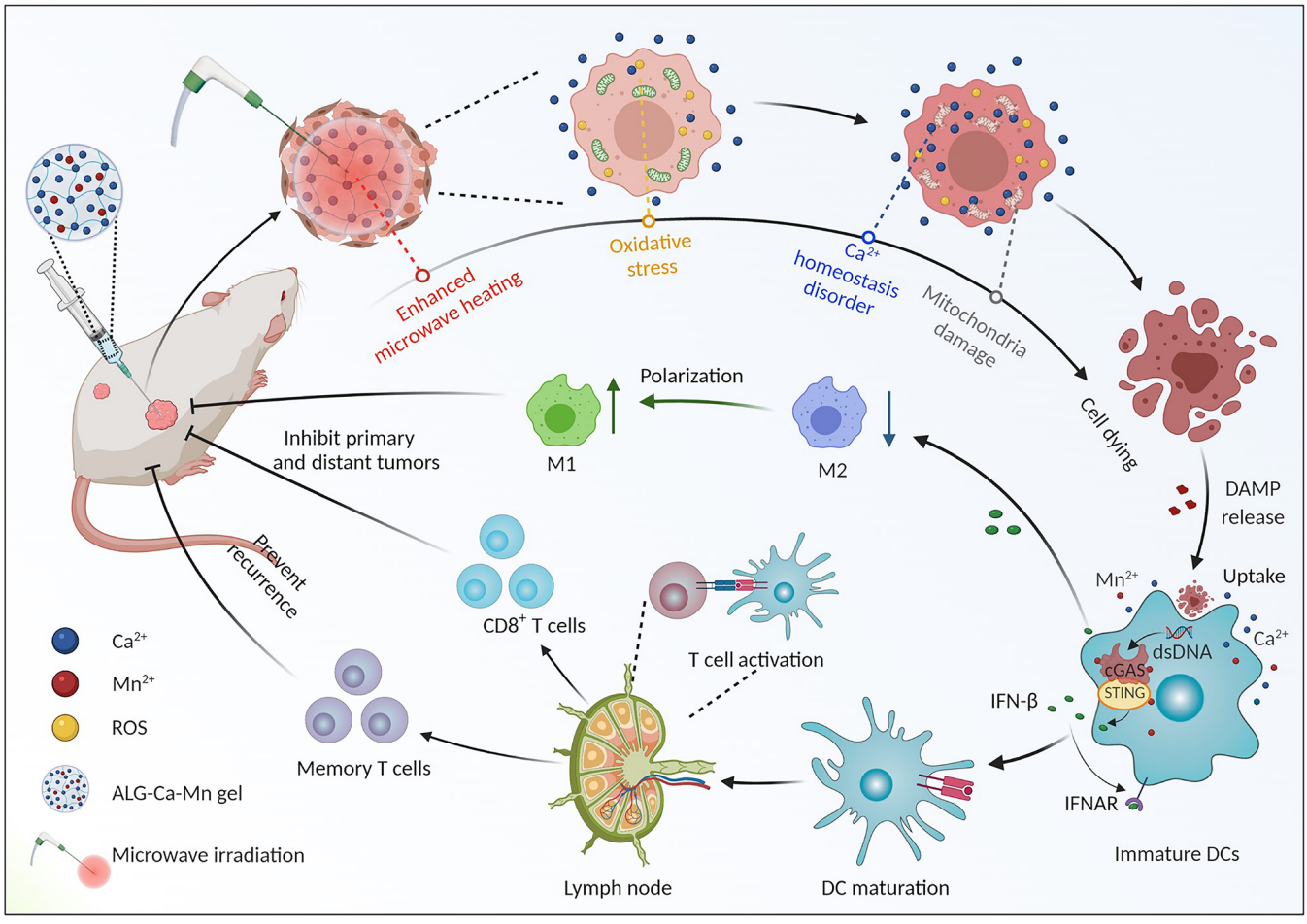

Fig. 1. A scheme illustrating the mechanism of metallo-alginate hydrogel in enhancing MWA treatment and boosting antitumor immunity. Upon being injected inside the tumors, this metallo-alginate hydrogel can work as a microwave heating sensitizer to enhance MWA of the primary tumor. Meanwhile, the existence of excess extracellular Ca^{2+} can sensitize cancer cells to mild thermal damage by disrupting intracellular calcium homeostasis, further promoting complete ablation of the primary tumor. In addition, the released DAMPs from these death cancer cells together with extracellular Ca^{2+} and Mn^{2+} would work together to prime effective innate and adaptive antitumor immune responses by activating the STING and other pathways to suppress the growth of both metastatic (distant) and relapsed (rechallenged) tumors. IFN-γ, interferon-γ; ROS, reactive oxygen species; DC, dendritic cell. IFNAR, interferon-α/β receptor.

treatment by activating the STING pathway. Therefore, this in situ–formed metallo-alginate hydrogel as a microwave susceptible and immunostimulatory agent would have great potential to assist clinically used MWA treatment.

RESULTS

Design and characterization of microwave susceptible Ca^{2+}-surplus alginate hydrogel

As a natural anionic polysaccharide, alginic acid and its salts [e.g., sodium alginate (ALG)] have been intensively used as pharmaceutical ingredients for diverse biomedical applications owing to their excellent biocompatibility (*28*). In particular, ALG could be used to enable in situ fixation of various payloads owing to its formation of hydrogels in the presence of endogenous Ca^{2+} ions (Fig. 2A). First, it was confirmed that ALG solution (20 mg ml^{-1}) appearing as viscous liquid would rapidly form hydrogel maintaining its integrity and shape in a slanted bottle upon being mixed with $CaCl_2$ (0.5 M) solutions (Fig. 2B). As indicated by the rheological behavior analysis, we found that as-prepared ALG hydrogels showed obvious ALG concentration–dependent storage modulus (Fig. 2C), solidly conforming the Ca^{2+}-triggered gelation property of ALG.

It has been reported that free-standing ions encapsulated within the small spaces of hydrogels, microcapsules, and hollow nanostructures can work as efficient microwave susceptible agents owing to the ion confinement effect (*17*, *18*). We therefore evaluated the microwave susceptibility of these ALG hydrogels (20 mg ml^{-1}) formed at varying Ca^{2+} concentrations (greater than, equal to, and less than the chelating capacity of ALG molecules) by recording their temperature increasing behaviors under microwave irradiation (5 W, 5 min). It was found that the ALG hydrogel formed at 0.5 M Ca^{2+} ions showed a rapid temperature increase of 20.7°C under this microwave irradiation, much higher than 7.8° and 5.9°C for ALG hydrogels formed at 0.05 and 0.005 M Ca^{2+} ions, respectively (Fig. 2D). Considering the saturated Ca^{2+} chelating capacity of ALG molecules at 20 mg ml^{-1} is theoretically equal to 0.05 M, these results imply that free-standing Ca^{2+} ions inside the as-prepared Ca^{2+}–cross-linking ALG hydrogel (coined as Ca^{2+}-surplus ALG

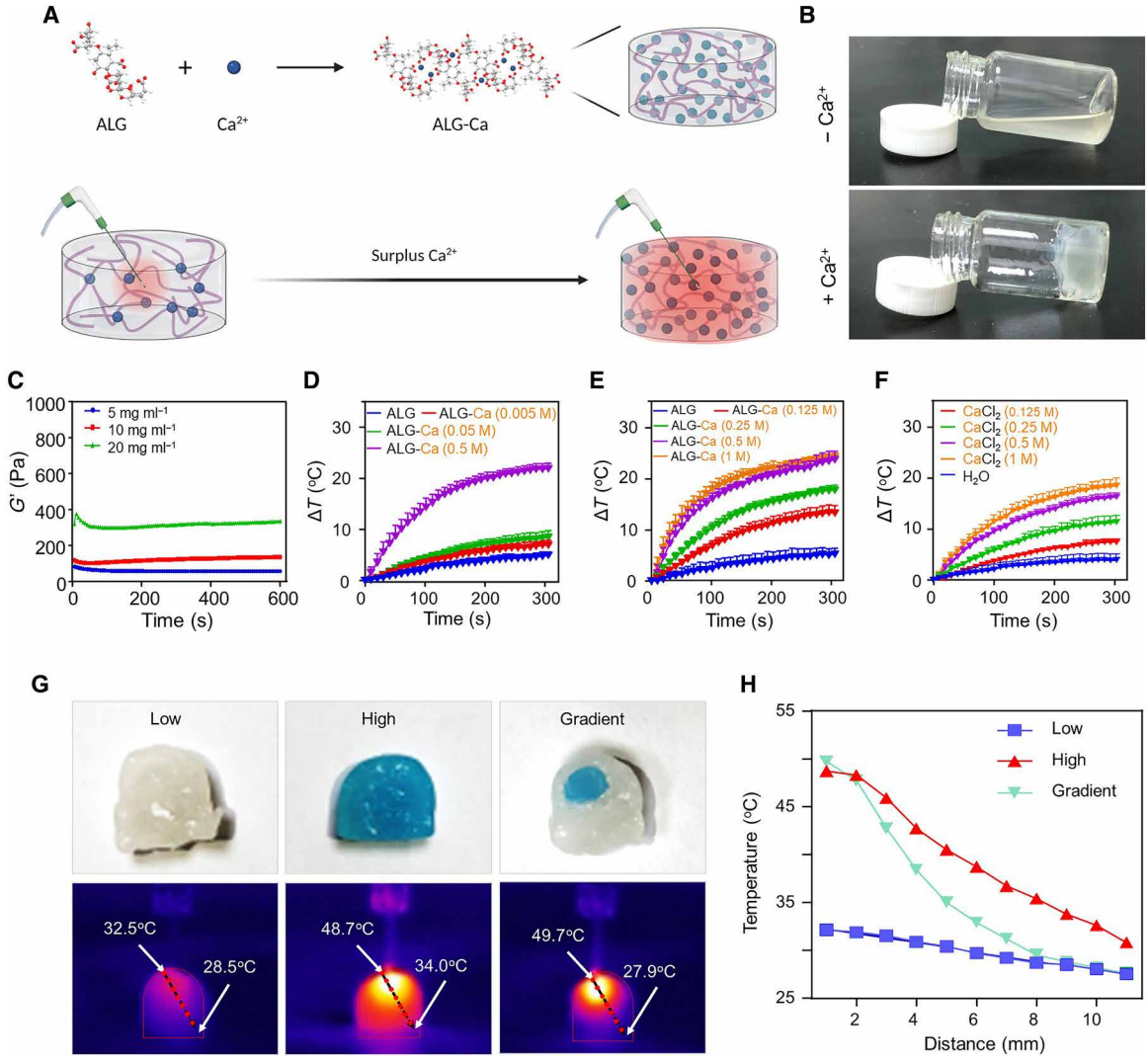

Fig. 2. Preparation and characterization of ALG-Ca gel. (**A**) A scheme illustrating the preparation of Ca^{2+}-surplus ALG hydrogel for enhanced microwave heating. (**B**) Optical images of ALG with/without Ca^{2+}. (**C**) Rheological behavior analysis of ALG-Ca gels with different ALG concentrations. (**D**) Microwave heating profiles of ALG solution and ALG-Ca hydrogel formed as varying concentrations of Ca^{2+} as indicated. (**E**) Microwave heating profiles of ALG solution and ALG-Ca hydrogel formed with ALG concentration (20 mg ml^{-1}) and Ca^{2+} ions at different concentrations as indicated. (**F**) Microwave heating profiles of $CaCl_2$ solutions at different concentrations. (**G** and **H**) Thermal images (G) and corresponding distance-dependent heating profiles of three types of ALG-Ca hydrogel with homogenous Ca^{2+} concentrations of 0.05 M (bottom, left) and 0.5 M (top, middle), and gradient Ca^{2+} concentrations (0.05 and 0.5 M, right). Methylene blue was used to indicated the high concentration of Ca^{2+}.

hydrogel) would function as an efficient microwave susceptible agents via the ion confinement effect (*17*, *29*). Furthermore, the microwave susceptibility of Ca^{2+}-surplus ALG hydrogels (ALG = 20 mg ml^{-1}) was shown to be in proportion to Ca^{2+} concentrations in range of 0.05 to 0.5 M (Fig. 2E) and much effective than bulk Ca^{2+} solutions at equivalent Ca^{2+} concentrations (Fig. 2F). Meanwhile, we observed that the ALG hydrogel formed with ALG (20 mg ml^{-1}) at Ca^{2+} ions (0.05 M) exhibited less effective microwave heating capacity than those formed with ALG at lower concentrations (5 and 10 mg ml^{-1}) in the presence of 0.05 M Ca^{2+} ions under the same microwave irradiation (fig. S1).

Next, we investigated the potency of Ca^{2+}-surplus ALG hydrogels to concentrate the microwave heating zone. To this end, three types of ALG hydrogels with gradient Ca^{2+} concentrations (0.05 and 0.5 M), homogenous low Ca^{2+} concentration (0.05 M) and homogenous high Ca^{2+} concentration (0.5 M) were prepared. Upon being exposed to a microwave irradiation (5 W, 5 min), we found that the hydrogel with homogenous low Ca^{2+} concentration showed an inconspicuous increase in temperature, while the hydrogel with homogenous high Ca^{2+} concentration showed a marked temperature increase. Meanwhile, the hydrogel with gradient Ca^{2+} concentrations showed rapid temperature increase only in the zone with the high Ca^{2+} concentration, but not in the surround region with the low concentration of Ca^{2+} (Fig. 2, G to H). Together, these results indicate that the Ca^{2+}-surplus ALG-Ca hydrogel is promising to concentrate the microwave heating zone to its injection site while leaving the surrounding tissues with free ions at physiological concentrations minimally disturbed.

Study of the immunogenic cell killing capacity of increased extracellular Ca^{2+} together with hyperthermia

As an important intracellular second messenger, both extracellular and intracellular concentrations of Ca^{2+} ions are precisely regulated to control various physiological processes including cell proliferation and survival (*30*–*32*). As a result, disruption of intracellular Ca^{2+} hemostasis has recently been shown to be a promising approach to kill cancer cells because the abnormal oscillation of intracellular Ca^{2+} concentration can activate a series of lethal signal transduction (*33*). Therefore, we carefully studied the impact of high-concentration extracellular Ca^{2+} exposure on the cell viability of cancer cells, particularly in the presence of mild hyperthermia, which has been reported to be capable of enhancing the therapeutic efficacy of diverse cancer therapies (*34*–*36*), by using the standard methyl thiazolyl tetrazolium (MTT) cell proliferation assay. We found that the viabilities of murine CT26 cells were minimally affected upon incubation with $CaCl_2$ at a series of Ca^{2+} concentrations at 37°C for up to 4 hours (Fig. 3A). In marked contrast, incubating CT26 cells with $CaCl_2$ (Ca^{2+} = 2 and 4 mM) at 43°C (mild hyperthermia) for 4 hours would result in notable cell death, although this mild hyperthermia treatment itself showed negligible influence on the viability of CT26 cells treated with $CaCl_2$ exposure at lower concentrations. Further increase of hyperthermia treatment temperature to 50°C, however, would kill most of cells regardless of $CaCl_2$ exposure. The ability of extracellular Ca^{2+} to enhance mild hypothermia mediated cell killing was further confirmed by the lactate dehydrogenase (LDH) leakage assay (fig. S2).

To further elucidate the mechanism of the observed synergistic cell killing capacity of increased extracellular $CaCl_2$ incubation under mild hyperthermia exposure, we then carefully evaluated the cell killing capacity of various different metal salts at 43°C toward CT26 cancer cells. It was found that the mild hyperthermia treatment negligibly affected the viabilities of CT26 cells incubated with NaCl, KCl, $MnCl_2$, and $ZnCl_2$ at varying concentrations (Fig. 3, B to D, and fig. S3). It was then shown that the mild hyperthermia exposure (43°C, 4 hours) with the addition of extracellular Ca^{2+} (4 mM) could also cause more effective death of murine H22 liver cancer cells and rabbit VX2 liver cancer cells (Fig. 3, E and F). In marked contrast, this combination treatment strategy showed negligible influence on normal human umbilical vein epithelial cells (fig. S4), which may be attributed to the lower intrinsic oxidative stress levels inside these normal cells than that of cancer cells (*37*). Collectively, our results demonstrated that the mild hyperthermia in the presence of a high concentration of extracellular Ca^{2+} could synergistically induce cancer cell death.

Next, we studied the mechanisms of extracellular Ca^{2+} plus mild hyperthermia to kill cancer cells. It has been reported that hyperthermia treatment (also known as heat shock) can promote intracellular reactive oxygen species (ROS) generation and disrupt intracellular Ca^{2+} homeostasis by promoting extracellular Ca^{2+} influx, thereby resulting in irreversible mitochondrial damages and cell death (*33*, *38*–*40*). Via the immunofluorescent staining, we found that the mild hyperthermia treatment (43°C, 4 hours) could lead to increased heat shock protein 70 (HSP70) expression inside treated CT26 cells as analyzed by both confocal microscopic observation and flow cytometric analysis (Fig. 3G and fig. S5). Consistently, we found that the mild hyperthermia could also effectively promote intracellular ROS generation using a cell-permeable ROS probe of 2′-7′-dichlorofluorescein diacetate (DCFH-DA; Fig. 3H and fig. S6). In contrast, CT26 cells treated by extracellular Ca^{2+} alone without hyperthermia showed negligible disturbance on the HSP70 expression and little ROS generation. Moreover, as indicated by using a fluorescent Ca^{2+} probe of Fluo-4AM, CT26 cells treated by simultaneous extracellular Ca^{2+} (4 mM) and mild hyperthermia (43°C) showed increased intracellular Ca^{2+} concentration (Fig. 3I and fig. S7), which, however, was not affected by extracellular Ca^{2+} incubation under normal temperature or mild hyperthermia alone without additional Ca^{2+}. As mitochondrial is an organelle playing a key role in regulating intracellular calcium homeostasis and its dysfunction would cause cell death (*41*), we then evaluated the effect of this combination treatment on the mitochondrial membrane potential of cells. After being stained with rhodamine 123, a potentiometric fluorescent dye used for assessing the electrochemical potential across mitochondrial membrane, we found that only cells simultaneously treated by extracellular Ca^{2+} and mild hyperthermia showed obvious fluctuation of mitochondrial membrane potential (Fig. 3J and fig. S8). These results demonstrated that mild hyperthermia treatment would lead to intracellular ROS generation, which synergizes with abundant extracellular Ca^{2+} ions influx to promote the elevation of intracellular Ca^{2+} and subsequent damage of mitochondrial membrane potential (Fig. 3K), further leading to irreversible cell death.

Next, we therefore carefully explored the potential immunostimulatory efficacy of this combination treatment by evaluating its potency in causing the release of diverse DAMPs including adenosine triphosphate (ATP), calreticulin (CRT), and high mobility group box 1 (HMGB1). Via the microscopic observation, we found that the mild hyperthermia exposure (43°C) in the presence of additional extracellular Ca^{2+} (4 mM) for 4 hours could result in the most effective expression of CRT on the plasma membrane and release of HMGB1 from the nuclei of CT26 cells, respectively. In marked contrast, the mild hyperthermia treatment alone showed moderate disturbance on the expression of CRT and release of HMGB1 of those treated cells, while the extracellular Ca^{2+} exposure alone minimally disturbed the expression of CRT and release of HMGB1 of those treated cells (Fig. 3, L and M). These results were consistent with corresponding flow cytometric analysis data (fig. S9). In addition, we found that CT26 cells treated by the mild hyperthermia exposure (43°C) with addition of extracellular Ca^{2+} (4 mM) for 4 hours resulted in the most effective ATP release, while the bare mild hyperthermia treatment (43°C) showed moderate effect on ATP release via the measurement with a commercial ATP detection kit (Fig. 3N). Given that CRT, HMGB1, and ATP have been recognized as typical biomarkers of ICD, our results collectively demonstrated that extracellular Ca^{2+} exposure could synergize with mild hyperthermia treatment to elicit effective ICD of cancer cells.

In vivo therapeutic efficacy of combined in situ Ca^{2+} fixation and MWA treatment

Considering that effective intratumoral retention of Ca^{2+} would offer a wide time window to enable high effective MWA treatment and avoid fast Ca^{2+} leakage induced side effect, we therefore carefully investigated the tumor retention profiles of these in situ fixed Ca^{2+} in the presence of ALG hydrogel. By using an inductively coupled plasma optical emission spectrometer (ICP-OES), it was determined that ~53.1% of these in situ–fixed Ca^{2+} remained at tumor site at 24 hours after injection, while only 26.8% of free Ca^{2+} intratumorally injected in the absence of ALG remained at tumor

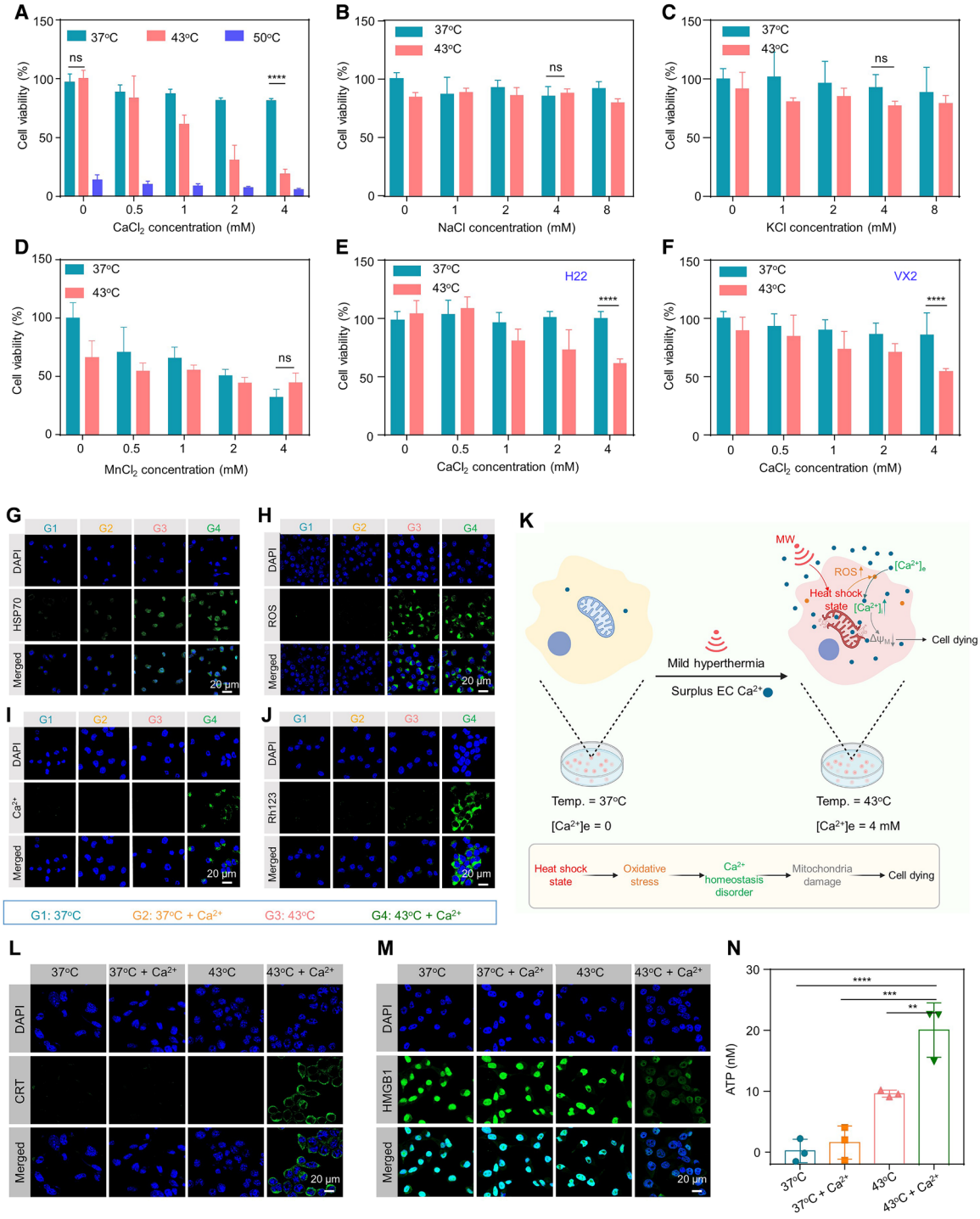

Fig. 3. Extracellar exposure of high concentration of Ca^{2+} potentiated the cancer cell killing of mild hyperthermia. (**A**) Relative cell viabilities of CT26 cells incubated with different concentrations of $CaCl_2$ at 37°, 43°, and 50°C. (**B** to **D**) Relative cell viabilities of CT26 cells incubated with different concentrations of NaCl (B), KCl (C), and $MnCl_2$ (D) at 37° and 43°C. (**E** and **F**) Relative viabilities of H22 (E) and VX2 (F) cells incubated with different concentrations of $CaCl_2$ at 37° and 43°C. (**G** to **J**) Confocal images of intracellular heat shock protein 70 (HSP70) expression (G), ROS generation (H), Ca^{2+} influx (I), and mitochondrial membrane potential change (J) of CT26 cells after various treatments. DAPI, 4API, s treatments.membrane po (**K**) Schematic illustration of the synergistic cell killing mechanism of increased extracellular $CaCl_2$ exposure in the presence of mild hyperthermia treatment. (**L** and **M**) Microscopic observation of CT26 cells with various treatments before being stained with calreticulin (CRT) antibody (L) and high mobility group box 1 (HMGB1) antibody (M). (**N**) Adenosine triphosphate (ATP) secretion assay of CT26 cells with varying treatments. Data were presented as the means ± SD. Statistical analysis was performed using one-way analysis of variance (ANOVA; ****$P < 0.0001$, ***$P < 0.001$, and **$P < 0.01$). ns, not significant.

site (Fig. 4A). In addition, it was found that the microwave exposure minimally affected the retention profile of these in situ–fixed Ca^{2+}, indicating that ALG hydrogel could enable effective intratumoral retention of Ca^{2+} ascribing to its excellent ion chelating capacity. Then, we investigated the in vivo microwave susceptibility of this in situ–formed Ca^{2+}-surplus ALG hydrogel on CT26 tumor–bearing mice. As recorded using a thermal infrared camera, it was shown that CT26 tumors with intratumoral injections of ALG (20 mg ml^{-1}) and $CaCl_2$ (0.5 M) showed rapid temperature increase and kept at ~42° and 50°C upon microwave exposure at the power densities of 3 and 5 W for 10 min, respectively. Whereas tumors with intratumoral injection of ALG (20 mg ml^{-1}) alone needed to be heated at higher power densities of 5 and 7 W for 10 min to achieve comparable microwave heating effects, respectively (Fig. 4, B and C). In marked contrast, CT26 tumors with intratumoral injection of $CaCl_2$ solutions (0.5 M) only exhibited limited temperature increase after being exposed to the microwave irradiation at 30 min after the injection (fig. S10), ascribing to the fast leakage of Ca^{2+} from tumor sites. Furthermore, it was uncovered that a large volume of Ca^{2+}-surplus ALG hydrogel (2 ml) could be easily injected into the porcine liver, used as the mimic of large tumors, and then enable a more rapid microwave heating and a larger thermal ablation volume (fig. S11). These results collectively demonstrate that the in situ–fixed Ca^{2+}-surplus ALG hydrogel could work as an effective microwave susceptible biomaterial.

Next, we evaluated the in vivo treatment efficacy of this ALG-Ca–assisted MWA treatment in subcutaneous CT26 tumor–bearing mice (Fig. 4D). When their tumor volumes reached ~100 cm^3, six groups of mice received following treatments: group 1, control group with saline injection; group 2, ALG-Ca hydrogel (0.5 M) injection only; group 3, ALG injection plus MWA (5 W); group 4, ALG injection plus MWA (7 W); group 5, ALG-Ca hydrogel (0.5 M) plus MWA (3 W); and group 6, ALG-Ca hydrogel (0.5 M) plus MWA (5 W). It was found that the treatments of groups 4 and 6, both of which could heat tumors to ~50°C, fully ablated treated tumors without noticeable tumor recurrence for up to 60 days

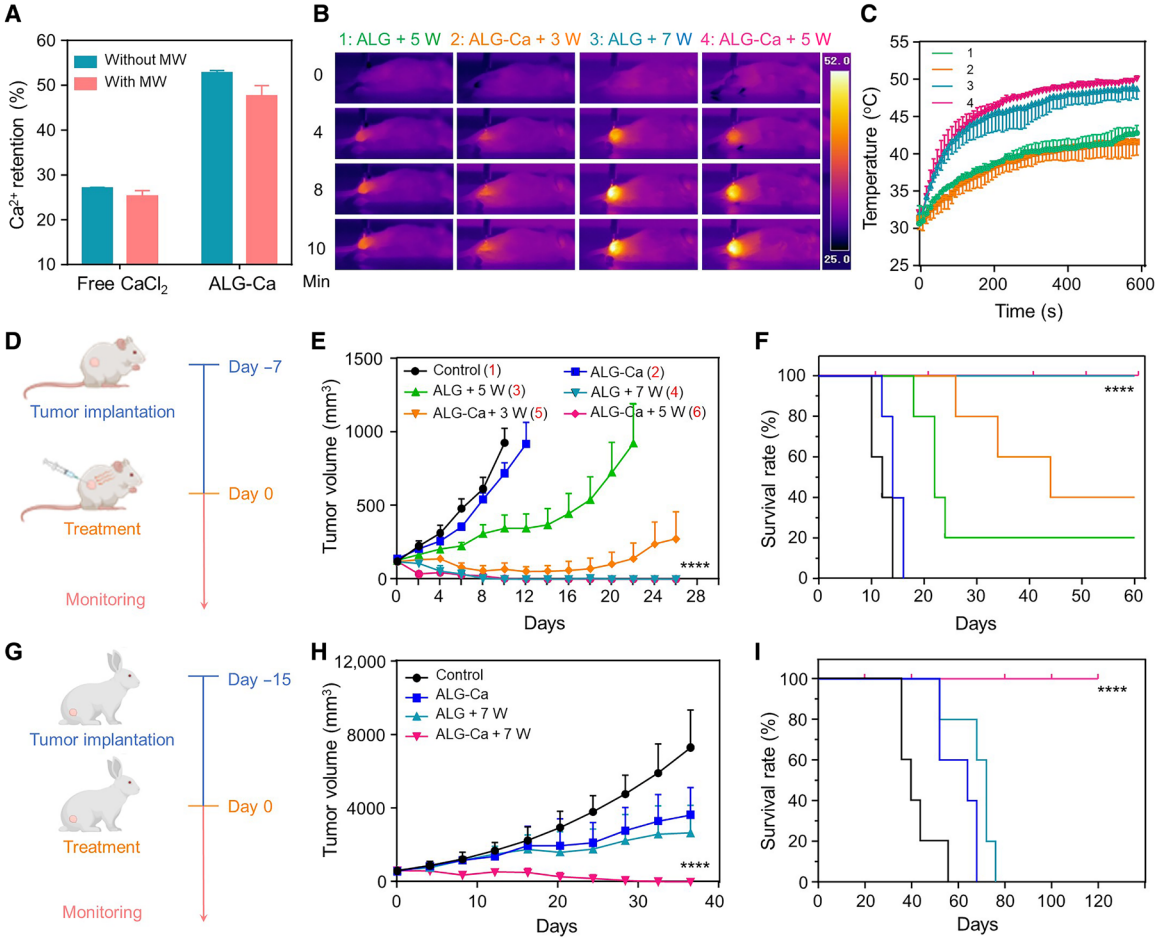

Fig. 4. In vivo ALG-Ca–assisted MWA treatment. (**A**) In vivo Ca^{2+} retention profiles of free $CaCl_2$ and ALG-Ca hydrogel with/without MWA. (**B** and **C**) Thermal images and microwave heating profiles of in vivo microwave susceptibility of ALG (20 mg ml^{-1}) and Ca^{2+}-surplus ALG-Ca hydrogel (20 mg ml^{-1}, 0.5 M). (**D**) Schematic illustration of the experimental schedule for subcutaneous CT26 tumor model treatment. (**E** and **F**) Tumor growth curves and corresponding mobility-free survival rate (F) of CT26 tumor–bearing mice post different treatments as indicated ($n = 5$). The mice were set as death when their tumor volume was larger than 1000 mm^3. (**G**) Schematic illustration of the subcutaneous VX2 tumor model treatment experimental schedule. (**H** and **I**) Tumor growth curves (H) and corresponding mobility-free survival rate (I) of VX2 tumor–bearing rabbits after different treatments as indicated ($n = 5$). The rabbits were set as death when their tumor volume was larger than 8000 mm^3. Data were presented as the means ± SEM. *P* values were calculated by using unpaired *t* test (****$P < 0.0001$).

(Fig. 4, E and F). The different power densities of microwave irradiation treatments here were used to ensure these treatments to achieve the complete ablation of primary tumors with varying injections. In addition, it was interestingly found that the treatment of ALG-Ca hydrogel injection and MWA at 3 W for 10 min (group 5) exhibited more effective tumor suppression effect than the treatment of plain ALG hydrogel injection and MWA at 5 W (group 3), although both treatments heated tumors to ~42°C. The median survival time of mice of group 5 was 44 days, much longer than 22 days for the mice in group 3, further confirming that the high concentration of extracellular Ca^{2+} could significantly enhance the therapeutic efficacy of mild hyperthermia as aforementioned in vitro cellular experimental results. Whereas the treatment of plain ALG-Ca hydrogel injection minimally influenced the growth rate of these treated tumors. The superior therapeutic efficacies of the treatments of groups 4 and 6 were further confirmed by the tumor slices collected at 24 hours after corresponding treatments and stained via the hematoxylin and eosin staining and terminal deoxynucleotidyl transferase–mediated deoxyuridine triphosphate nick end labeling staining (fig. S12). These results demonstrated that in situ fixation of high concentration of Ca^{2+} could effectively enhance the therapeutic efficacy of MWA, particularly against tumor cells in the zone at a subtherapeutic temperature.

Furthermore, we investigated the therapeutic potency of ALG-Ca–assisted MWA treatment on large subcutaneous VX2 tumors grown on New Zealand rabbits (Fig. 4G). Four groups of VX2 tumor–bearing rabbits were (volume = ~700 mm^3, $n = 5$) treated as below: group 1, saline injection only; group 2, ALG-Ca hydrogel (0.5 M) injection only; group 3, ALG injection plus MWA (7 W); and group 4, ALG-Ca hydrogel (0.5 M) injection plus MWA (7 W). As expected, these VX2 tumors treated with ALG-Ca injection plus MWA exposure (10 min, group 4) were completely ablated and no obvious recurrence ware observed in the following 120-day monitoring process (Fig. 4, H and I). In contrast, the treatments of ALG-Ca hydrogel injection alone (group 2) and ALG injection plus MWA (group 3) only moderately delayed the tumor growth with their median survival times quantified to be 64 and 72 days, respectively, much longer than 40 days for these untreated rabbits. Our results further confirmed the high therapeutic efficacy of our combined treatment of in situ fixation of Ca^{2+}-surplus ALG hydrogel and MWA exposure.

Study of combined in situ Ca^{2+} fixation and MWA treatment boosted antitumor immunity

As a critical second messenger in immune cell signaling, it has been reported that Ca^{2+} itself can work as dangerous signals to activate dendritic cells (DCs) via different mechanisms (*42*). With the bone marrow–derived DCs (BMDCs) as the model, we found that the increased extracellular Ca^{2+} incubation could significantly promote the maturation of BMDCs as indicated by the increased expressions of surface markers of CD80 and CD86 via the flow cytometric analysis (fig. S13). Together with their high efficacy in promoting the release of immunostimulatory DAMPs, we investigated the potency of this combined in situ fixation of Ca^{2+}-surplus ALG hydrogel and MWA exposure in inhibiting the growth of distant untreated and rechallenged tumors by activating the host's antitumor immunity (Fig. 5A).

First, five groups of mice with two CT26 tumors on their both flanks ($n = 5$) were treated as below: group 1, saline injection only; group 2, ALG-Ca hydrogel (0.5 M) injection; group 3, ALG injection plus MWA (7 W); group 4, ALG + R837 (15 mg kg^{-1}) injection plus MWA (7 W) group; and group 5, ALG-Ca hydrogel injection plus MWA (5 W). The large tumors in these bilateral CT26 tumor–bearing mice received same treatment as aforementioned apart from group 4, in which R837 (imiquimod), a TLR7 agonist, was introduced to enhance the immunostimulatory effect after ALG-Ca–assisted MWA treatment. Consistent to the aforementioned in vivo treatment results, the treatments of groups 3 to 5 were shown to be capable of fully ablating primary tumors, while the treatment of group 2 showed limited inhibitory effect on the growth of treated tumor (Fig. 5B). We found that the treatment in group 5 showed effective suppression effect on the growth of these untreated distant tumor, comparable to the treatment of group 4 with R837 as the immunostimulatory agonist (Fig. 5C). Whereas the treatments of groups 2 and 3 only exhibited moderate suppression effect on the growth of these treated mice without significant extension of mouse survival time (Fig. 5D). Meanwhile, ALG-Ca–assisted MWA treatment was shown to be safe at the tested dosed as it would not cause significant weight loss of these treated mice (Fig. 5E). These results demonstrated that the ALG-Ca–assisted MWA treatment could effectively suppress the growth of distant tumors, the mimic of metastatic tumors, via eliciting potent abscopal effects.

The detailed mechanisms of this ALG-Ca–assisted MWA treatment in eliciting potent abscopal effects were then carefully investigated. Therefore, another six groups of bilateral CT26 tumor models ($n = 5$) were treated as below: group 1, saline injection only; group 2, ALG-Ca hydrogel injection; group 3, ALG injection + MWA irradiation (7 W) group; group 4, ALG-R837 injection; group 5, ALG-R837 injection + MWA (7 W); and group 6, ALG-Ca hydrogel injection + MWA (5 W). The different power densities of microwave irradiation treatments here were used to ensure these treatments to achieve the complete ablation of primary tumors with varying injections. At 7 days after varying treatments of their large tumors (day 7), these mice were euthanized with distant tumors and their lymph nodes adjacent to primary tumors collected, homogenized, and stained with varying antibodies by flow cytometric analysis. It was notably found that our ALG-Ca–assisted MWA treatment could effectively activate DCs inside the lymph nodes by promoting their maturation, at comparable efficacy to the treatment of ALG-R837 injection plus MWA (group 5; Fig. 5F and fig. S14). Meanwhile, the ALG-Ca–assisted MWA treatment could also remarkably increase the abundances of total $CD3^+$ T cells and $CD3^+CD8^+$ T cells inside the distant tumors at a comparable level to the treatment of group 5 (Fig. 5, G and H, and fig. S15). Although these treatments negligibly affected the abundances of immunosuppressive regulatory T cells (T_{regs}) inside distant tumors of mice, we found that the ALG-Ca–assisted MWA treatment (group 6) could result in comparable increase of $CD3^+CD8^+$ T cells/T_{reg} ratios (Fig. 5I and fig. S16), an important sign of activation of host's antitumor immunity to the treatment of group 5 with R837 plus MWA. Moreover, it was uncovered that the ALG-Ca–assisted MWA treatment in group 6 could also lead to efficient secretion of cytotoxic cytokines of tumor necrosis factor–α (TNF-α) and interferon-γ (IFN-γ) inside distant tumors at comparable levels to the R837-assisted MWA treatment in group 5 (Fig. 5, J and K). These results indicated that ALG-Ca–assisted MWA is able to create a locoregional proinflammatory microenvironment to benefit the recruitment of immune cells and thus potentiate the host's

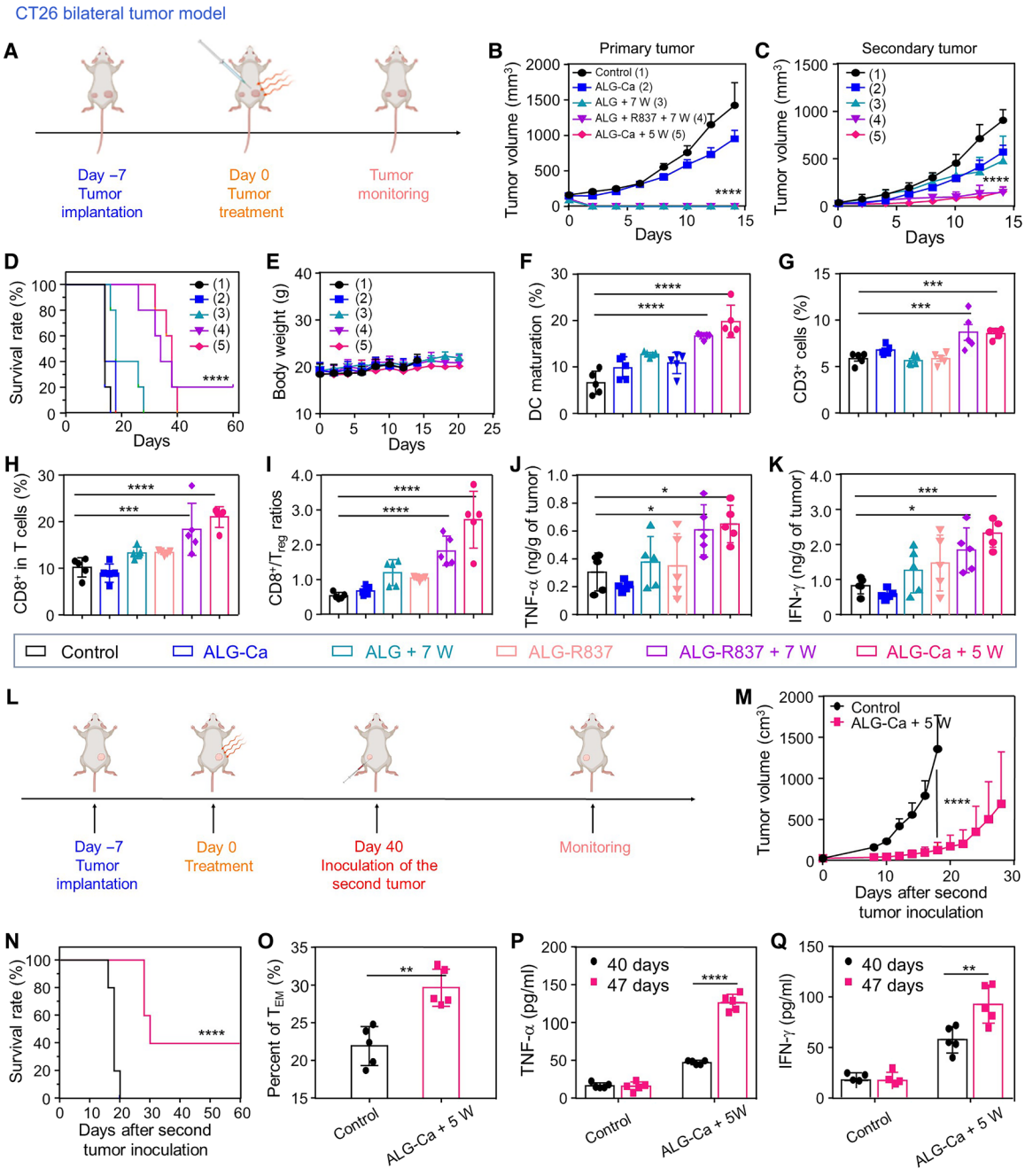

Fig. 5. ALG-Ca–assisted MWA treatment in eliciting antitumor immunity. (**A**) Schematic illustration of the utilization of bilateral CT26 tumor model for in vivo antitumor treatment. (**B** to **E**) Tumor growth curves of primary (B) and distant tumors (C), as well as corresponding mobility-free survival rate (D) and body weights (E) of mice with their large tumors after different treatments as indicated ($n = 5$). The mouse was set as death when its tumor volume was large than 1000 mm^3. (1), (2), (3), (4), (5) represent Control, ALG-Ca, ALG+7W, ALG+R837+7W and ALG-Ca+5W, respectively. (**F**) DC maturation status in the drain lymph nodes adjacent to the primary tumors post various treatments as indicated. (**G** to **I**) The frequencies of $CD3^+$ cells (G), $CD3^+CD8^+$ T cells (H), and the ratios of $CD3^+CD8^+$ T cells to corresponding regulatory T cells (T_{regs}) inside the distant tumors after various treatments as indicated. (**J** and **K**) The secretion levels of tumor necrosis factor–α (TNF-α) (J) and IFN-γ (K) inside the distant tumors after various treatments as indicated. (**L**) Schematic illustration of the tumor rechallenge assay. (**M** and **N**) Tumor growth curves (M) and mobility-free survival rate (N) of mice after various treatments as indicated ($n = 5$). (**O**) Proportions of effector T memory (T_{EM}) analyzed by flow cytometry at day 40, right before rechallenging mice with secondary tumors. (**P** and **Q**) Cytokine levels including TNF-α (P) and IFN-γ (Q) in sera from mice isolated right before and 7 days after mice were rechallenged with secondary tumors. Data were represented as means ± SEM ($n = 5$ biologically independent animals). *P* values in (B) to (D) and (M) to (Q) were calculated by using unpaired *t* test (*$P < 0.05$, **$P < 0.01$, and ***$P < 0.001$). *P* values in (F) to (K) were calculated by using one-way ANOVA (*$P < 0.05$, **$P < 0.01$, ***$P < 0.001$, and ****$P < 0.0001$).

antitumor immunity. Besides, this Ca^{2+}-surplus ALG hydrogel itself could work as a potent immune adjuvant biomaterial at a comparable immunostimulatory potency to commercial R837 at the tested dose to further reinforce the activation of antitumor immunity. Considering that R837 is prone to cause unwanted immune stimulation–related side effects if diffused out from the injection site, our Ca^{2+}-surplus ALG hydrogel holds superior biocompatibility because both Ca^{2+} and ALG themselves in the absence of hyperthermia treatment would not cause any obvious side effects.

As another hallmark of the activation of host's antitumor immune responses, immunological memory induced by diverse cancer treatments can provide long-term protective effect to inhibit tumor recurrence (*43*, *44*). Therefore, the potency of ALG-Ca–assisted MWA treatment in preventing tumor recurrence were then carefully assessed on a tumor challenge model. To this end, CT26 tumor–bearing mice cured by ALG-Ca–assisted MWA were subcutaneously injected with CT26 cells at 40 days after the initial MWA treatment, while another group of healthy mice were also injected with CT26 cells as the control (Fig. 5L). We observed that the growth rate of tumors inoculated in the cured mice was much slower than that in the control mice, and two of the five cured mice were able to completely reject the growth of rechallenged second tumors (Fig. 5, M and N). Furthermore, by flow cytometric analysis, the abundance of effector T memory ($CD3^+CD8^+CD44^+CD62L^-$cells in the peripheral blood collected from the cured mice before the inoculation of second CT26 tumors were determined to be 29.7%, significantly higher than 21.9% in the healthy mice (Fig. 5O and fig. S17). By using the enzyme-linked immunosorbent assays (ELISAs), the serum levels of TNF-α and IFN-γ collected from these cured mice at 7 days after the secondary CT26 tumor inoculation (day 47) were much higher than those detected at day 40 before tumor inoculation (Fig. 5, P to Q). In sharp contrast, these control mice showed the comparable secretion levels of TNF-α and IFN-γ in their sera at the aforementioned two time points. Collectively, these results demonstrated that ALG-Ca–assisted MWA could elicit potent immune memory effect to reject tumor recurrence.

Study of the potency of in situ Ca^{2+} and Mn^{2+} fixation in potentiating MWA treatment

In recent years, the effect of metal ions on antitumor immunity has been widely reported. In particular, Mn^{2+} ions have been proven to be capable of eliciting effective innate and adaptive antitumor immunities by activating the STING pathway (*45*, *46*). Motivated by the high affinity of ALG in binding diverse divalent metal ions, we therefore prepared a Mn^{2+}-loaded Ca^{2+}-surplus ALG hydrogel (Ca^{2+}/Mn^{2+}-surplus ALG hydrogel) and then explored its potency in potentiating MWA treatment by activating the antitumor immune responses. First, it was confirmed that the encapsulated Mn^{2+} ions would be gradually released from the Ca^{2+}/Mn^{2+}-surplus ALG hydrogel and promote the activation of the STING pathway inside BMDCs in a concentration-dependent manner (fig. S18). Next, via the flow cytometric analysis, the mixture of Ca^{2+} (4 mM) and Mn^{2+} (200 μM) was further found to be more effective than Ca^{2+} and Mn^{2+} alone in promoting the maturation of BMDCs (Fig. 6A and fig. S19). Meanwhile, it was determined that incubation with Ca^{2+} and Mn^{2+} together or Mn^{2+} alone could result in effective secretion of IFN-β, a characteristic cytokine of the STING pathway activation, at a comparable level from treated BMDCs (Fig. 6B). In marked contrast, incubation with Ca^{2+} alone minimally affected the IFN-β secretion. In addition, the high STING activation capacity of Mn^{2+} was confirmed on commercial 293-Dual mSTING reporter cells (ISG-SEAP/KI-[IFN-β]Lucia) by measuring the released Lucia luciferase activity using a QUANTI-Luc luciferase detection reagent (Fig. 6, C and D). These results demonstrated that both extracellular exposure of high concentration of Ca^{2+} ions (4 mM) and Mn^{2+} ions can promote DC maturation, while only Mn^{2+} ions can activate the STING pathway. Therefore, the induction of Mn^{2+} ions is expected to synergize with the ALG-Ca–assisted MWA treatment to prime a more potent antitumor immune response.

Therefore, the potency of this Ca^{2+}/Mn^{2+}-surplus ALG hydrogel in potentiating MWA treatment was evaluated on a poorly immunogenic murine H22 liver tumor model with two tumors inoculated on their both flanks (Fig. 6E). Then, six groups of these bilateral H22 tumor models (control group, $n = 6$; the rest of groups, $n = 8$; large tumor = ~100 mm^3 and small tumor = ~30 mm^3) were treated as below: group 1, saline injection only; group 2, ALG-Ca injection; group 3, ALG-Ca-Mn injection; group 4, ALG injection + MWA (7 W); group 5, ALG-Ca injection + MWA (5 W); and group 6, ALG-Ca-Mn injection + MWA (5 W). These large tumors of mice received same ALG-Ca fixation and MWA treatment as aforementioned, and Mn^{2+} was injected at a dose of 7 mg/kg. As expected, we observed that the addition of Mn^{2+} could further enhance the therapeutic efficacy of ALG-Ca–assisted MWA treatment in suppressing the growth of untreated distant tumors (Fig. 6, F and G, and fig. S20). The survival rate of mice treated with ALG-Ca-Mn–assisted MWA was determined to be 37.5%, significantly higher than 12.5% for these mice treated with ALG-Ca–assisted MWA (Fig. 6H). Although Mn^{2+} has been reported be able to induce potential toxic effect, our combination treatment with Ca^{2+}/Mn^{2+}-surplus ALG hydrogel and MWA did not cause significant body weight loss (fig. S21), indicating its good biocompatibility at the tested dose.

The detailed mechanism of this ALG-Ca-Mn–assisted MWA treatment in eliciting potent abscopal effects was then carefully investigated as aforementioned. Another six groups of bilateral H22 tumor models ($n = 6$) received same treatments as above mentioned at day 0 and then were euthanized at day 7 for various analysis. Notably, the ALG-Ca-Mn–assisted MWA treatment resulted in the most effective DC maturation inside lymph nodes close to treated tumors (Fig. 6I and fig. S22). As the result, this ALG-Ca-Mn–assisted MWA treatment could also contribute to the highest tumor-infiltrating $CD3^+CD8^+$ T cell abundance and $CD3^+CD8^+$ T cell/T_{reg} ratio (Fig. 6, J and K, and fig. S23), implying the effective priming of adaptive antitumor immunity. It was also shown that the treatment could effectively promote the intratumoral abundance of proinflammatory M1 macrophages, while leading to a slight reduction of anti-inflammatory M2 ones (Fig. 6, L to N, and figs. S24 and S25). This significantly primed innate antitumor immunity could be ascribed to the activation of the STING pathway, verified by the increased expression of IFN-γ inside the distant tumors (Fig. 6O), as previously reported (*47*, *48*). Furthermore, it was uncovered that ALG-Ca-Mn–assisted MWA could also lead to the highest secretion levels of diverse inflammatory cytokines including IFN-γ, TNF-α, interleukin-12p70 (IL-12p70), and IL-6 inside the distant tumors by using corresponding ELISA kits (Fig. 6, P to S). These results collectively implied that the introduction of Mn^{2+} is able to effectively potentiate the immunostimulatory capacity of ALG-Ca-Mn–assisted MWA by activating the STING pathway.

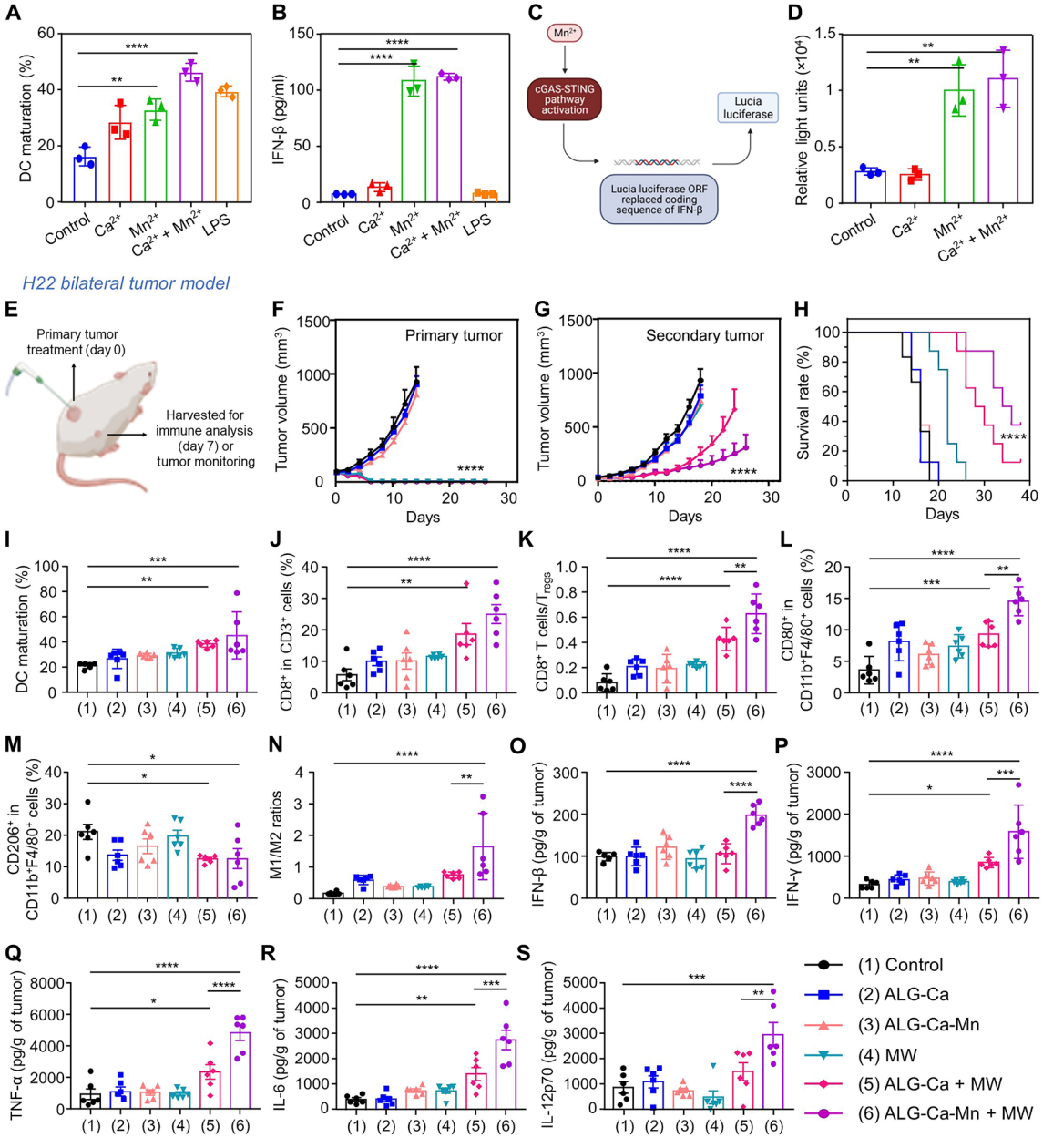

Fig. 6. The potency of ALG-Ca-Mn to enhance MWA treatment of H22 tumor model. (**A** and **B**) Maturity rate (A) and IFN-β secretion levels of BMDC cells with various treatments via the flow cytometry and ELISA assay, respectively. (**C**) Schematic illustration of the working principle of 293-Dual mSTING reporter cells. (**D**) Relative light units (RLU) of 293-Dual mSTING cells transfected with cGAS plasmid with varying treatmentsfor 24 hours before being measured using a QUANTI-Luc luciferase detection kit. (**E**) Schematic illustration of the experimental schedule on subcutaneous H22 bilateral tumor model. (**F** to **H**) The tumor growth curves of primary tumors (F) and distant tumors (G), as well as mobility-free survival rate (H) of H22 tumor–bearing mice after different treatments as indicated (control group, $n = 6$; the other groups, $n = 8$). The mice were set as death when their tumor volume was larger than 1000 mm^3. (**I**) DC maturation status in the drain lymph nodes adjacent to the primary tumors after various treatments as indicated. (**J** to **N**) The intratumoral frequencies of $CD3^+CD8^+$ T cells (J), the ratios of $CD3^+CD8^+$ T cells to corresponding T_{regs} (K), intratumoral frequencies of $CD11b^+F4/80^+/CD80^+$ M1 cells (L) and $CD11b^+F4/80^+/CD206^+$ M2 cells (M), and the ratios of M1/M2 (N) inside the distant tumors of mice after various treatments as indicated. (**O** to **S**) The secretion levels of IFN-β (O), IFN-γ (P), TNF-α (Q), IL-6 (R), and IL-12p70 (S) inside the distant tumors of mice with varying treatments as indicated. Data were represented as means ± SEM. *P* values in (F) to (H) were calculated by using unpaired *t* test (*$P < 0.05$, **$P < 0.01$, and ***$P < 0.001$). *P* values in (A), (B), (D), and (I) to (S) were calculated by using one-way ANOVA (*$P < 0.05$, **$P < 0.01$, ***$P < 0.001$, and ****$P < 0.0001$).

Biocompatibility evaluation of ALG-ca-Mn–assisted MWA treatment

We then evaluated the biocompatibility of our proposed therapeutic regimen of ALG-Ca-Mn–assisted MWA treatment because the high exposure doses of Ca^{2+} and Mn^{2+} ions might cause some unwanted side effects. Via the biochemical blood test and routine blood test, we found that both ALG-Ca-Mn–assisted and ALG-Ca–assisted MWA treatments following the aforementioned therapeutic regimens negligibly impair the concentration of urea in the blood (fig. S26A), revealing that they would not significantly damage the

normal functions of the kidneys throughout the 14-day monitoring process. On the other side, although high concentration of Ca^{2+} in the blood is prone to cause the blood coagulation by promoting the contraction of platelets (*49*), we confirmed that our treatments did not obviously impair the function of platelets because the index of mean platelet volume of treated mice was minimally disturbed (fig. S26B). Furthermore, we uncovered that these treatments also minimally disturb the normal functions of red blood cells (fig. S26, C to L). Together with the results shown in fig. S21 that these treatments did not affect the body weights of treated mice, we demonstrated that our proposed ALG-Ca-Mn–assisted MWA treatment would be rather safe and thus hold great promise for future clinical translation.

DISCUSSION

In this study, we prepared a metallo-alginate hydrogel with promising microwave susceptibility and immunostimulatory effect to potentiate MWA treatment. Attributing to the high loading capacity of alginate polymer to diverse divalent metal ions, traditional ALG hydrogel could be used as a concise platform to enable in situ fixation of different metal ions under the guidance of real-time imaging instruments (e.g., ultrasonography) for varying purposes. Using its tunable microwave susceptibility by adjusting the concentrations of free-standing Ca^{2+} ions and ALG, the in situ–formed Ca^{2+}-surplus ALG hydrogel could not only enable effective microwave heating at a reduced power density but also concentrate the heat inside the injected zone, thereby showing great promise to reduce the side effects faced by the conventional MWA treatment. Together with the high potency of high extracellular Ca^{2+} exposure in enhancing the cell killing ability of the subtherapeutic hyperthermia (e.g., 43°C) by destructing intracellular Ca^{2+} homeostasis, our proposed ALG-Ca–assisted MWA treatment could offer superior therapeutic efficacy.

Furthermore, owing to the ability of extracellular Ca^{2+} in potentiating mild hyperthermia mediated release of diverse immunostimulatory DAMPs, this in situ–formed Ca^{2+}-surplus ALG hydrogel was found to be a potent adjuvant biomaterial to promote the maturation of DCs at a comparable immunostimulatory potency to commercial R837. Moreover, by virtue of the high capacity of ALG hydrogels in loading divalent metal ions (e.g., STING activating Mn^{2+}), the simultaneous introduction of Mn^{2+} could further enhance the immunostimulatory capacity of MWA treatment by activating the STING pathway. Therefore, ALG-Ca–assisted MWA, especially ALG-Ca-Mn–assisted MWA with the addition of Mn^{2+} ions, could effectively delay the growth of both distant and rechallenged tumors, showing great promises to inhibit tumor metastasis and prevent tumor recurrence.

In summary, this study presents the concise preparation of a type of metallo-alginate hydrogel as a bifunctional biomaterial to potentiate conventional MWA treatment by enhancing the microwave heating efficacy and priming efficient antitumor immunity. Together with its excellent biocompatibility and easy operation, this metallo-alginate hydrogel holds great promises for future clinical translation to extend the clinical application of MWA treatment.

MATERIALS AND METHODS

Materials

ALG was obtained from J&K Chemicals. $CaCl_2$ was obtained from Sigma-Aldrich. Manganese chloride ($MnCl_2$), sodium chloride (NaCl), zinc chloride ($ZnCl_2$), and potassium chloride (KCl) were purchased from Sinopharm Chemical Reagent Co. RPMI 1640 medium (no calcium nitrate) was purchased from HyClone. Antibodies for flow cytometric analysis of intratumoral immune cells were obtained from BioLegend and eBioscience. ELISA kits were obtained from Invitrogen.

Preparation and characterization of Ca^{2+}-surplus ALG hydrogel

Ca^{2+}–cross-linked ALG hydrogels (ALG-Ca) with varying ALG contents were prepared by mixing $CaCl_2$ aqueous solutions at designated concentrations with equivalent volume of ALG aqueous solution at different concentrations. The elastic modulus (G') and viscous modulus (G'') of ALG-Ca hydrogel formed with ALG (5, 10, and 20 mg ml^{-1}) and $CaCl_2$ (0.5 M) were determined by using an Anton Paar rheometer.

To evaluate the microwave susceptibility, the as-prepared ALG-Ca hydrogels at different ALG (5, 10, and 20 mg ml^{-1}) and Ca^{2+} concentrations (0.005, 0.125, 0.25, 0.5, and 1 M) were exposed to a microwave probe (5 W, 2.45 GHz; WB-3100, BXING MEDICAL EQUIPMENT CO. LTD.) for 5 min, and their surface temperatures were recorded by using thermal infrared camera (Fotric 225). For parallel comparison, the temperature evolution profiles of both ALG solution and Ca^{2+} solutions at varying concentrations under the same microwave exposure were also recorded as aforementioned.

To demonstrate the potency of the Ca^{2+}-surplus ALG hydrogel in concentrating the heating zone, a small ALG-Ca hydrogel with high Ca^{2+} concentration (0.5 M) obtained by mixing ALG solution (40 mg ml^{-1}, 300 μl) with $CaCl_2$ solution (1 M, 300 μl) were mounted within another ALG-Ca hydrogel with low Ca^{2+} concentration (0.05 M, 4 ml). Apart from this hydrid ALG-Ca hydrogel, other ALG-Ca hydrogel with homogenous Ca^{2+} concentrations at 0.5 or 0.05 M in similar shapes were then prepared as the control groups. Later, these three hydrogels were exposed to a microwave irradiation (5 W, 2.45 GHz) for 5 min, and their heating profiles were recorded by using a thermal infrared camera as aforementioned.

Cell experiments

Murine CT26 colon cancer cells (TCM37), H22 hepatocellular carcinoma cells (ZQ0109), and rabbit VX2 liver cancer cells (MZ-0769) were obtained from the Cell Bank of Shanghai Institutes for Biological Sciences, Shanghai Zhongqiao Xinzhou Biological Technology Co. Ltd., and Ningbo Mingzhou Biological Technology Co. Ltd., respectively. These cells were maintained under the standard culture conditions.

To study the Ca^{2+} exposure enhanced hyperthermia mediated cell killing, CT26 cells were preseeded in 96-well cell culture plates (1×10^4 cells) overnight and then incubated with $CaCl_2$ solutions at varying Ca^{2+} concentrations for 4 hours at 37°, 43°, and 50°C before their relative viabilities were determined by using the standard MTT assay. Meanwhile, culture medium of each well was collected with the released LDH measured using a commercial LDH detection kit. In addition, the same experimental procedures were applied on H22 and VX2 cells. To study the influence of mild hyperthermia treatment on the cytotoxicity of other metal ions, these preseeded CT26 cancer cells were treated with other salts including KCl, NaCl, $ZnCl_2$, and $MnCl_2$ via the aforementioned procedure. To test the effects of hyperthermia treatment on HSP70 expression, preseeded CT26 cells (1×10^5 cells) were incubated with the fresh RPMI 1640

containing varying concentrations of $CaCl_2$ (0 and 4 mM) at 37° or 43°C for 4 hours. Then, the treated CT26 cells were sequentially stained with HSP70 primary antibody (dilution, 1:500), corresponding secondary antibody (dilution, 1:500), and 4′,6-diamino-2-phenylindole (1 μg ml^{-1}) before being subjected to confocal microscopic observation (Zeiss, LSM 800). In addition, the HSP70 expression levels of CT26 cells with same treatments were subjected to quantitative flow cytometric analysis (BD Accurit C6 Plus).

Then, CT26 cells with same treatments were washed twice with phosphate-buffered saline (PBS) before being incubated with of DCFH-DA (10 μM and 30 min), Fluo-4AM (2 μM and 30 min), and rhodamine 123 (2 μM and 30 min) for determining their intracellular ROS production, Ca^{2+} internalization and mitochondria damage via the confocal microscopic observation and flow cytometric analysis, respectively.

To test the cellular ATP release, the supernatants of these cells with same treatments as aforementioned were collected to determine their ATP concentrations by using an ATP assay kit. CT26 cells received same treatments were stained with anti-CRT (catalog no. ab2907, Abcam) and anti-HMGB1 (catalog no. 70-ab40050-100, Abcam) primary antibodies and their corresponding fluorescent secondary antibodies (catalog no. 111-545-003, Jackson) for evaluating the CRT expression and HMGB1 release via the microscopic observation and flow cytometry, respectively.

To test the influence of Ca^{2+} on DCs maturation, BMDCs differentiated from bone marrow cells of C57BL/6 mice were prepared by according to an established method (*50*). Then, BMDCs were seeded in 24-well nontreated plates (1×10^6 cells) and then incubated with different concentrations of Ca^{2+} or lipopolysaccharide (LPS) for 15 hours before being stained with fluorescent antibodies against CD11c, CD86, and CD80 for 30 min and analyzed via the flow cytometry. The influence of Mn^{2+} on DC maturation was tested through the same method. In this experiment, BMDCs incubated with blank medium, Ca^{2+} (2 mM), Mn^{2+} (200 μM), Ca^{2+}/Mn^{2+} (2 mM, 200 μM), and LPS for 15 hours.

Animal experiments

Female Balb/c mice, Balb/c nude mice, and specific pathogen–free New Zealand white rabbits were purchased from Laboratory Animal Center of Soochow University and used by following the protocols approved by Laboratory Animal Center of Soochow University. To inoculate subcutaneous tumor models, CT26 cells (2×10^6) or H22 cells (2×10^6) suspended in 50 μl of PBS were subcutaneously injected to the back of each mouse. To inoculate bilateral tumor models, 1×10^6 and 2.5×10^5 CT26 or H22 cells were simultaneously injected into right and left flanks of each mouse, respectively. To inoculate the rabbit tumor model, small pieces of VX2 tumor mass collected from the Balb/c nude mice were injected into the back of each rabbit. Tumor size was calculated as follows: volume = (tumor length) × (tumor width)^2/2.

In vivo Ca^{2+} retention

Twelve CT26 tumor–bearing mice were randomly divided to two groups and received intratumoral injection of ALG (40 mg ml^{-1}, 25 μl) and $CaCl_2$ (1 M, 25 μl) or free $CaCl_2$ (1 M, 25 μl) alone. Thirty minutes later, three mice of each group were randomly picked out and subjected to microwave irradiation (5 W, 10 min), followed by collecting their tumors at 24 hours after injection to determine the intratumoral Ca^{2+} contents with ICP-OES. The rest of the three mice of each group without microwave irradiation were also euthanized with their tumors collected for determining the Ca contents with ICP-OES.

In vivo cancer treatment

Six groups of CT26 tumor–bearing Balb/c mice received the following treatments: group 1, saline; group 2, ALG-Ca; group 3, ALG + MWA (5 W, 10 min); group 4, ALG + MWA (7 W, 10 min); group 5, ALG-Ca + MWA (3 W, 10 min); and group 6, ALG-Ca + MWA (5 W, 10 min). The intratumoral injection doses of ALG and $CaCl_2$ were 40 mg $ml^{-1}$and 1 M at equivalent volume of 25 μl, and the operation frequency of microwave irradiator was 2.45 GHz as aforementioned. The tumor surface temperature of these mice during the microwave exposure was measured by using a thermal camera (Fotric 225). The tumor volume and body weight of each mouse was monitored by using the digital caliper and balance every other day.

In addition, four groups of VX_2 tumor–bearing New Zealand white rabbits received the following treatments: group 1, saline; group 2, ALG-Ca; group 3, ALG + MWA (7 W, 10 min); and group 4, ALG-Ca + MWA (7 W, 10 min). The injection dosages of diverse agent for the VX_2 rabbit tumor model were 10-fold of those used for the mouse models. Their tumor length and width were recorded as aforementioned for determined tumor volume.

Abscopal effect of ALG-Ca–assisted MWA treatment

When their large tumors reached ~100 mm^3, five groups of bilateral CT26 tumor–bearing mice received the following treatments: group 1, saline; group 2, ALG-Ca; group 3, ALG + MWA (7 W, 10 min); group 4, ALG-R837 + MWA (7 W, 10 min, R837 = 15 mg kg^{-1}); and group 5, ALG-Ca + MWA (5 W, 10 min). These mice were received intratumoral injections of ALG and $CaCl_2$ at the aforementioned doses before being exposed to microwave irradiation. Then, the sizes of both tumors on the each mouse and their body weights were also recorded as aforementioned.

Then, the detailed antitumor immune responses of these mice after various treatments were carefully analyzed. Six groups of bilateral CT26 tumor model (n = 5) received the following treatments: group 1, saline; group 2, ALG-Ca; group 3, ALG + MWA (7 W); group 4, ALG + R837; group 5, ALG-R837 + MWA (7 W); and group 6, ALG-Ca + MWA (5 W). At 7 days after various treatments at the aforementioned doses, the lymph nodes close to the treated tumors and untreated tumors of these mice were collected for preparing single-cell suspensions by following our previously used procedures (*10*). After being stained with varying fluorescent antibodies, the percentages of maturated DCs ($CD11c^+CD80^+CD86^+$), total $CD3^+$ T cells, $CD8^+$ T cells ($CD3^+CD4^-CD8^+$), and T_{regs} ($CD3^+CD4^+Foxp3^+$) were analyzed by using the flow cytometry. Then, the intratumoral contents of IFN-γ and TNF-α of homogenized tumor suspensions were determined using corresponding ELISA kits under the manufacturer's procedures.

Immune memory effect of ALG-Ca–assisted MWA treatment

For evaluating the long-term immune memory effect induced by the ALG-Ca–assisted MWA treatment, these cured mice were rechallenged with the same CT26 cells (2×10^6 cells) at 40 days after the primary treatments. Meanwhile, five healthy mice were subcutaneously injected with same CT26 cancer cells as the control group. The sizes of these rechallenged tumors were monitored as

aforementioned. In addition, the peripheral blood of each mouse (~200 μl) was collected at day 40 before the inoculation of the second tumor and day 47 for analyzing the percentage of memory T cell via flow cytometry and the cytokines of TNF-α and IFN-γ via the ELISA assay.

The potency of ALG-Ca-Mn–assisted MWA to treat H22 tumor model

Six groups of bilateral H22 tumor models (control group, $n = 6$; the rest of groups, $n = 8$) received the following treatments: group 1, saline; group 2, ALG-Ca injection; group 3, ALG-Ca-Mn injection; group 4, ALG injection + MWA (7 W); group 5, ALG-Ca injection + MWA (5 W); and group 6, ALG-Ca-Mn injection + MWA (5 W). These mice received the same ALG-Ca fixation and MWA treatment as aforementioned, and Mn^{2+} (7 mg/kg) was simultaneously injected. The sizes of these untreated distant tumors and the body weights were also monitored as aforementioned.

Then, the detailed antitumor immune responses of these mice after various treatments were carefully analyzed. Six groups of mice received various treatments as aforementioned were euthanized at 7 after the treatment for preparing single-cell suspensions of lymph nodes close to the treated tumors and untreated tumors as aforementioned. The frequencies of maturated DCs ($CD11c^+CD80^+CD86^+$), $CD8^+$ T cells ($CD3^+CD4^-CD8^+$), T_{regs} ($CD3^+CD4^+Foxp3^+$), M1 ($CD11b^+F4/80^+CD80^+$), and M2 ($CD11b^+F4/80^+CD206^+$) were analyzed via the flow cytometry. Then, the secretion levels of IFN-γ, TNF-α, IL-6, IL-12p70, and IFN-β of these tumor lysates were analyzed using corresponding ELISA kits as aforementioned.

SUPPLEMENTARY MATERIALS

Supplementary material for this article is available at https://science.org/doi/10.1126/sciadv.abo5285

View/request a protocol for this paper from *Bio-protocol*.

REFERENCES AND NOTES

1. C. J. Simon, D. E. Dupuy, W. W. Mayo-Smith, Microwave ablation: Principles and applications. *RadioGraphics* **25**, S69–S83 (2005).
2. X. Wu, B. Liu, B. Xu, Theoretical evaluation of high frequency microwave ablation applied in cancer therapy. *Appl. Therm. Eng.* **107**, 501–507 (2016).
3. P. Liang, X. L. Yu, J. Yu, *Microwave Ablation Treatment of Solid Tumors* (Springer, 2014).
4. T. J. Vogl, L. M. Basten, N.-E. A. Nour-Eldin, B. Kaltenbach, B. Bodelle, J. L. Wichmann, H. Ackermann, N. N. N. Naguib, Evaluation of microwave ablation of liver malignancy with enabled constant spatial energy control to achieve a predictable spherical ablation zone. *Int. J. Hyperthermia* **34**, 492–500 (2018).
5. T. Livraghi, F. Meloni, L. Solbiati, G. Zanus; Collaborative Italian Group using AMICA system, Complications of microwave ablation for liver tumors: Results of a multicenter study. *Cardiovasc. Intervent. Radiol.* **35**, 868–874 (2012).
6. S. Qin, G.-J. Liu, M. Huang, J. Huang, Y. Luo, Y. Wen, Y. Wang, L. Chen, The local efficacy and influencing factors of ultrasound-guided percutaneous microwave ablation in colorectal liver metastases: A review of a 4-year experience at a single center. *Int. J. Hyperthermia* **36**, 36–43 (2019).
7. Q. Zhou, N. Gong, D. Zhang, J. Li, X. Han, J. Dou, J. Huang, K. Zhu, P. Liang, X.-J. Liang, J. Yu, Mannose-derived carbon dots amplify microwave ablation-induced antitumor immune responses by capturing and transferring "Danger Signals" to dendritic cells. *ACS Nano* **15**, 2920–2932 (2021).
8. X. Han, R. Wang, J. Xu, Q. Chen, C. Liang, J. Chen, J. Zhao, J. Chu, Q. Fan, E. Archibong, L. Jiang, C. Wang, Z. Liu, In situ thermal ablation of tumors in combination with nano-adjuvant and immune checkpoint blockade to inhibit cancer metastasis and recurrence. *Biomaterials* **224**, 119490 (2019).
9. K. Leuchte, E. Staib, M. Thelen, P. Gödel, A. Lechner, P. Zentis, M. Garcia-Marquez, D. Waldschmidt, R. R. Datta, R. Wahba, C. Wybranski, T. Zander, A. Quaas, U. Drebber, D. L. Stippel, C. Bruns, M. von Bergwelt-Baildon, K. Wennhold, H. A. Schlößer, Microwave ablation enhances tumor-specific immune response in patients with hepatocellular carcinoma. *Cancer Immunol. Immunother.* **70**, 893–907 (2021).
10. Z. Yang, Y. Zhu, Z. Dong, W. Li, N. Yang, X. Wang, L. Feng, Z. Liu, Tumor-killing nanoreactors fueled by tumor debris can enhance radiofrequency ablation therapy and boost antitumor immune responses. *Nat. Commun.* **12**, 4299 (2021).
11. Y. Chao, C. Liang, H. Tao, Y. Du, D. Wu, Z. Dong, Q. Jin, G. Chen, J. Xu, Z. Xiao, Q. Chen, C. Wang, J. Chen, Z. Liu, Localized cocktail chemoimmunotherapy after in situ gelation to trigger robust systemic antitumor immune responses. *Sci. Adv.* **6**, eaaz4204 (2020).
12. Q. Chen, L. Xu, C. Liang, C. Wang, R. Peng, Z. Liu, Photothermal therapy with immune-adjuvant nanoparticles together with checkpoint blockade for effective cancer immunotherapy. *Nat. Commun.* **7**, 13193 (2016).
13. Q. Wu, N. Xia, D. Long, L. Tan, W. Rao, J. Yu, C. Fu, X. Ren, H. Li, L. Gou, P. Liang, J. Ren, L. Li, X. Meng, Dual-functional supernanoparticles with microwave dynamic therapy and microwave thermal therapy. *Nano Lett.* **19**, 5277–5286 (2019).
14. Q. Wu, J. Yu, M. Li, L. Tan, X. Ren, C. Fu, Z. Chen, F. Cao, J. Ren, L. Li, P. Liang, Y. Zhang, X. Meng, Nanoengineering of nanorattles for tumor treatment by CT imaging-guided simultaneous enhanced microwave thermal therapy and managing inflammation. *Biomaterials* **179**, 122–133 (2018).
15. C. Fu, H. Zhou, L. Tan, Z. Huang, Q. Wu, X. Ren, J. Ren, X. Meng, Microwave-activated Mn-doped zirconium metal–organic framework nanocubes for highly effective combination of microwave dynamic and thermal therapies against cancer. *ACS Nano* **12**, 2201–2210 (2018).
16. H. Shi, T. Liu, C. Fu, L. Li, L. Tan, J. Wang, X. Ren, J. Ren, J. Wang, X. Meng, Insights into a microwave susceptible agent for minimally invasive microwave tumor thermal therapy. *Biomaterials* **44**, 91–102 (2015).
17. Q. Du, C. Fu, J. Tie, T. Liu, L. Li, X. Ren, Z. Huang, H. Liu, F. Tang, L. Li, X. Meng, Gelatin microcapsules for enhanced microwave tumor hyperthermia. *Nanoscale* **7**, 3147–3154 (2015).
18. J. Wang, D. Wang, H. Yan, L. Tao, Y. Wei, Y. Li, X. Wang, W. Zhao, Y. Zhang, L. Zhao, X. Sun, An injectable ionic hydrogel inducing high temperature hyperthermia for microwave tumor ablation. *J. Mater. Chem. B* **5**, 4110–4120 (2017).
19. Q. Du, T. Ma, C. Fu, T. Liu, Z. Huang, J. Ren, H. Shao, K. Xu, F. Tang, X. Meng, Encapsulating ionic liquid and Fe_3O_4 nanoparticles in gelatin microcapsules as microwave susceptible agent for MR imaging-guided tumor thermotherapy. *ACS Appl. Mater. Interfaces* **7**, 13612–13619 (2015).
20. J. An, K. Zhang, B. Wang, S. Wu, Y. Wang, H. Zhang, Z. Zhang, J. Liu, J. Shi, Nanoenabled disruption of multiple barriers in antigen cross-presentation of dendritic cells via calcium interference for enhanced chemo-immunotherapy. *ACS Nano* **14**, 7639–7650 (2020).
21. D. L. Medina, A. Ballabio, Lysosomal calcium regulates autophagy. *Autophagy* **11**, 970–971 (2015).
22. G. Chan, D. J. Mooney, Ca^{2+} released from calcium alginate gels can promote inflammatory responses in vitro and in vivo. *Acta Biomater.* **9**, 9281–9291 (2013).
23. M. Zhang, R. Song, Y. Liu, Z. Yi, X. Meng, J. Zhang, Z. Tang, Z. Yao, Y. Liu, X. Liu, W. Bu, Calcium-overload-mediated tumor therapy by calcium peroxide nanoparticles. *Chem* **5**, 2171–2182 (2019).
24. S. K. Frandsen, H. Gissel, P. Hojman, T. Tramm, J. Eriksen, J. Gehl, Direct therapeutic applications of calcium electroporation to effectively induce tumor necrosis. *Cancer Res.* **72**, 1336–1341 (2012).
25. M. Du, Z. J. Chen, DNA-induced liquid phase condensation of cGAS activates innate immune signaling. *Science* **361**, 704–709 (2018).
26. C. Wang, R. Zhang, X. Wei, M. Lv, Z. Jiang, Metalloimmunology: The metal ion-controlled immunity. *Adv. Immunol.* **145**, 187–241 (2020).
27. D. Cen, Q. Ge, C. Xie, Q. Zheng, J. Guo, Y. Zhang, Y. Wang, X. Li, Z. Gu, X. Cai, ZnS@BSA nanoclusters potentiate efficacy of cancer immunotherapy. *Adv. Mater.* **33**, 2104037 (2021).
28. Y. Chao, L. Xu, C. Liang, L. Feng, J. Xu, Z. Dong, L. Tian, X. Yi, K. Yang, Z. Liu, Combined local immunostimulatory radioisotope therapy and systemic immune checkpoint blockade imparts potent antitumour responses. *Nat. Biomed. Eng.* **2**, 611–621 (2018).
29. Y. Cao, Y. Zhou, J. Pan, X. Zhong, J. Ding, X. Jing, S.-K. Sun, A general strategy towards an injectable microwave-sensitive immune hydrogel for combined percutaneous microwave ablation and immunotherapy. *Chem. Eng. J.* **422**, 130111 (2021).
30. H. L. Roderick, S. J. Cook, Ca2+ signalling checkpoints in cancer: Remodelling Ca2+ for cancer cell proliferation and survival. *Nat. Rev. Cancer* **8**, 361–375 (2008).
31. A. A. Peters, M. J. G. Milevskiy, W. C. Lee, M. C. Curry, C. E. Smart, J. M. Saunus, L. Reid, L. da Silva, D. L. Marcial, E. Dray, M. A. Brown, S. R. Lakhani, S. J. Roberts-Thomson, G. R. Monteith, The calcium pump plasma membrane Ca2+-ATPase 2 (PMCA2) regulates breast cancer cell proliferation and sensitivity to doxorubicin. *Sci. Rep.* **6**, 25505 (2016).
32. M. C. X. Pinto, A. H. Kihara, V. A. M. Goulart, F. M. P. Tonelli, K. N. Gomes, H. Ulrich, R. R. Resende, Calcium signaling and cell proliferation. *Cell. Signal.* **27**, 2139–2149 (2015).
33. S. Orrenius, B. Zhivotovsky, P. Nicotera, Regulation of cell death: The calcium–apoptosis link. *Nat. Rev. Mol. Cell Biol.* **4**, 552–565 (2003).
34. Y. Lv, F. Li, S. Wang, G. Lu, W. Bao, Y. Wang, Z. Tian, W. Wei, G. Ma, Near-infrared light–triggered platelet arsenal for combined photothermal-immunotherapy against cancer. *Sci. Adv.* **7**, eabd7614 (2021).

35. X. Liu, J. Zheng, W. Sun, X. Zhao, Y. Li, N. Gong, Y. Wang, X. Ma, T. Zhang, L.-Y. Zhao, Y. Hou, Z. Wu, Y. Du, H. Fan, J. Tian, X.-J. Liang, Ferrimagnetic vortex nanoring-mediated mild magnetic hyperthermia imparts potent immunological effect for treating cancer metastasis. *ACS Nano* **13**, 8811–8825 (2019).
36. M. Chang, Z. Hou, M. Wang, C. Li, J. Lin, Recent advances in hyperthermia therapy-based synergistic immunotherapy. *Adv. Mater.* **33**, 2004788 (2021).
37. C. M. Doskey, V. Buranasudja, B. A. Wagner, J. G. Wilkes, J. Du, J. J. Cullen, G. R. Buettner, Tumor cells have decreased ability to metabolize H2O2: Implications for pharmacological ascorbate in cancer therapy. *Redox Biol.* **10**, 274–284 (2016).
38. P. M. Harari, D. J. M. Fuller, E. W. Gerner, Heat shock stimulates polyamine oxidation by two distinct mechanisms in mammalian cell cultures. *Int. J. Radiat. Oncol. Biol. Phys.* **16**, 451–457 (1989).
39. J. Yu, F. Liu, P. Yin, H. Zhao, W. Luan, X. Hou, Y. Zhong, D. Jia, J. Zan, W. Ma, B. Shu, J. Xu, Involvement of oxidative stress and mitogen-activated protein kinase signaling pathways in heat stress-induced injury in the rat small intestine. *Stress* **16**, 99–113 (2013).
40. G. Ermak, K. J. A. Davies, Calcium and oxidative stress: From cell signaling to cell death. *Mol. Immunol.* **38**, 713–721 (2002).
41. G. Kroemer, J. C. Reed, Mitochondrial control of cell death. *Nat. Med.* **6**, 513–519 (2000).
42. M. Rossol, M. Pierer, N. Raulien, D. Quandt, U. Meusch, K. Rothe, K. Schubert, T. Schöneberg, M. Schaefer, U. Krügel, S. Smajilovic, H. Bräuner-Osborne, C. Baerwald, U. Wagner, Extracellular Ca2+ is a danger signal activating the NLRP3 inflammasome through G protein-coupled calcium sensing receptors. *Nat. Commun.* **3**, 1329 (2012).
43. Y. D. Mahnke, J. Schwendemann, P. Beckhove, V. Schirrmacher, Maintenance of long-term tumour-specific T-cell memory by residual dormant tumour cells. *Immunology* **115**, 325–336 (2005).
44. R. S. Goldszmid, J. Idoyaga, A. I. Bravo, R. Steinman, J. Mordoh, R. Wainstok, Dendritic cells charged with apoptotic tumor cells induce long-lived protective CD4 + and CD8 + T cell immunity against B16 melanoma. *J. Immunol.* **171**, 5940–5947 (2003).
45. C. Wang, Y. Guan, M. Lv, R. Zhang, Z. Guo, X. Wei, X. Du, J. Yang, T. Li, Y. Wan, X. Su, X. Huang, Z. Jiang, Manganese increases the sensitivity of the cGAS-STING pathway for double-stranded DNA and is required for the host defense against DNA viruses. *Immunity* **48**, 675–687.e7 (2018).
46. M. Lv, M. Chen, R. Zhang, W. Zhang, C. Wang, Y. Zhang, X. Wei, Y. Guan, J. Liu, K. Feng, M. Jing, X. Wang, Y.-C. Liu, Q. Mei, W. Han, Z. Jiang, Manganese is critical for antitumor immune responses via cGAS-STING and improves the efficacy of clinical immunotherapy. *Cell Res.* **30**, 966–979 (2020).
47. M. Takahashi, C.-W. J. Lio, A. Campeau, M. Steger, F. Ay, M. Mann, D. J. Gonzalez, M. Jain, S. Sharma, The tumor suppressor kinase DAPK3 drives tumor-intrinsic immunity through the STING–IFN-β pathway. *Nat. Immunol.* **22**, 485–496 (2021).
48. M. J. White, K. McArthur, D. Metcalf, R. M. Lane, J. C. Cambier, M. J. Herold, M. F. van Delft, S. Bedoui, G. Lessene, M. E. Ritchie, D. C. S. Huang, B. T. Kile, Apoptotic caspases suppress mtDNA-induced STING-mediated type I IFN production. *Cell* **159**, 1549–1562 (2014).
49. W. S. Nesbitt, S. Giuliano, S. Kulkarni, S. M. Dopheide, I. S. Harper, S. P. Jackson, Intercellular calcium communication regulates platelet aggregation and thrombus growth. *J. Cell Biol.* **160**, 1151–1161 (2003).
50. L. Xu, Y. Liu, Z. Chen, W. Li, Y. Liu, L. Wang, L. Ma, Y. Shao, Y. Zhao, C. Chen, Morphologically virus-like fullerenol nanoparticles act as the dual-functional nanoadjuvant for HIV-1 vaccine. *Adv. Mater.* **25**, 5928–5936 (2013).

Acknowledgments: We thank the website of app.Biorender.com for the assistance in creating the illustration figures. **Funding:** This work was supported by the National Natural Science Foundation of China (22077093 and 52032008), National Research Programs from Ministry of Science and Technology (MOST) of China (2021YFF0701800), Jiangsu Social Development Project (BE2019658), Collaborative Innovation Center of Suzhou Nano Science and Technology, and Suzhou Key Laboratory of Nanotechnology and Biomedicine 111 Program from the Ministry of Education of China. **Author contributions:** Conceptualization: Y.Z., L.F., and Z.L. Methodology: Y.Z. and L.F. Investigation: Y.Z., Z.Y., Z.P., Y.H., C.W., Z.D., Q.L., Y.H., and L.T. Supervision: L.F. and Z.L. Writing—original draft: Y.Z., L.F., and Z.L. Writing—review and editing: Y.Z., L.F., and Z.L. **Competing interests:** The authors declare that they have no competing interests. **Data and materials availability:** All data needed to evaluate the conclusions in the paper are present in the paper and/or the Supplementary Materials.

Submitted 10 February 2022
Accepted 16 June 2022
Published 3 August 2022
10.1126/sciadv.abo5285